Supporting Information

Lateral Heterostructures of Multilayer GeS and SnS van der Waals Crystals

Eli Sutter,[1] Jia Wang,[1] and Peter Sutter[2,*]

[1]*Department of Mechanical and Materials Engineering, University of Nebraska-Lincoln, Lincoln, Nebraska 68588 (USA)*
[2]*Department of Electrical and Computer Engineering, University of Nebraska-Lincoln, Lincoln, Nebraska 68588 (USA)*

1. Supplementary Figures

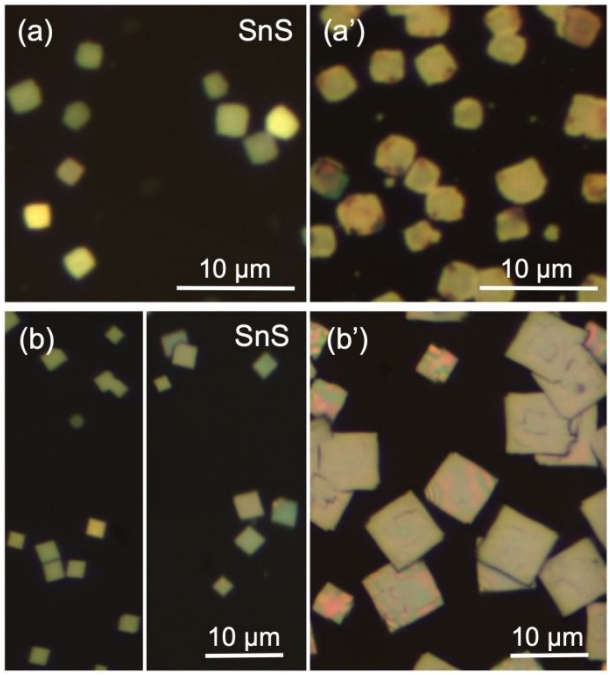

Figure S1. Morphology of SnS flakes and SnS-GeS heterostructures. (a), (b) Overview optical images of typical SnS flakes on mica substrates. **(a'), (b')** Optical images of the samples shown in (a) and (b), following additional GeS growth performed at source temperatures of 400°C and 450°C, respectively.

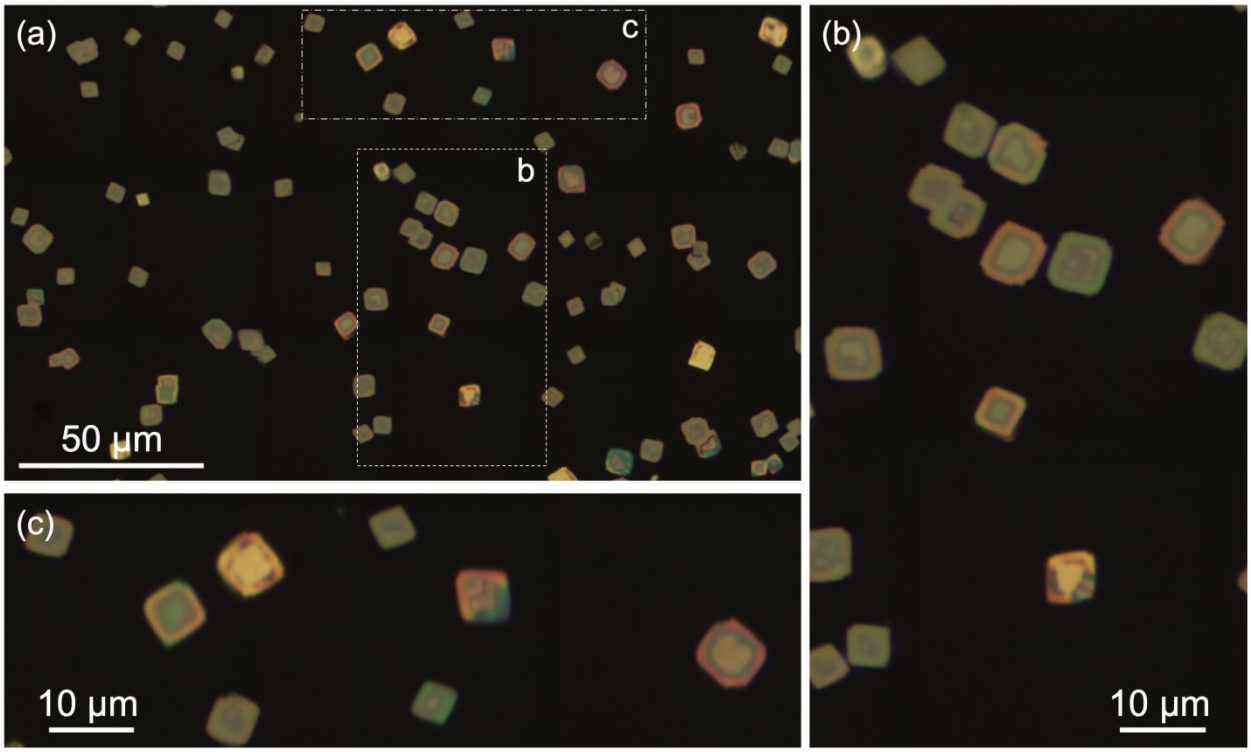

Figure S2. Heterogeneous attachment of GeS to SnS flakes, and overall yield of SnS-GeS heterostructures. (a) Overview optical image of typical SnS-GeS heterostructure flakes on mica substrate, formed with a second growth step at 320°C sample temperature and 420°C GeS source temperature. **(b), (c)** Zoomed-in optical images of the areas marked by dashed (b) and dash-dotted (c) rectangles in (a). Note the varying optical contrast due to the different flake thickness and differences between the optical constants of GeS and SnS. We find that no pure GeS flakes were (homogeneously) nucleated in the second growth step, and that each of the SnS seed flakes was converted into a heterostructure. We conclude that the areal density of heterostructures is determined by that of the SnS seed flakes, and that the yield of converting SnS seeds to SnS-GeS heterostructures is near unity.

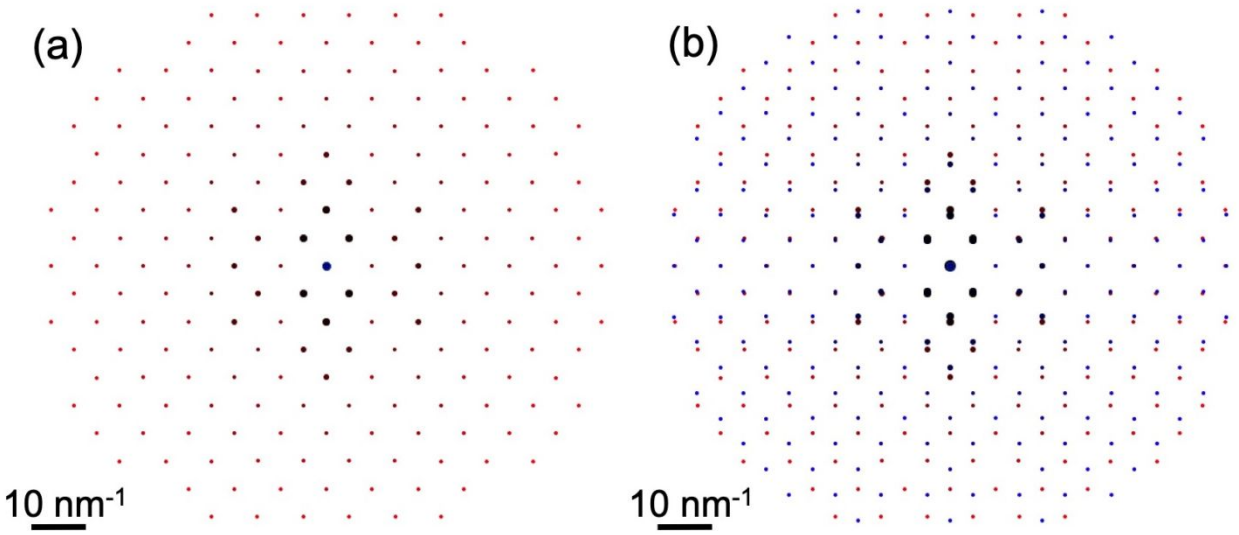

Figure S3. Simulated electron diffraction patterns along the [001] zone axis of **(a)** GeS, **(b)** superimposed GeS (red) and SnS (blue) with aligned in-plane (*a*, *b*) axes and their native (relaxed) lattice parameters.

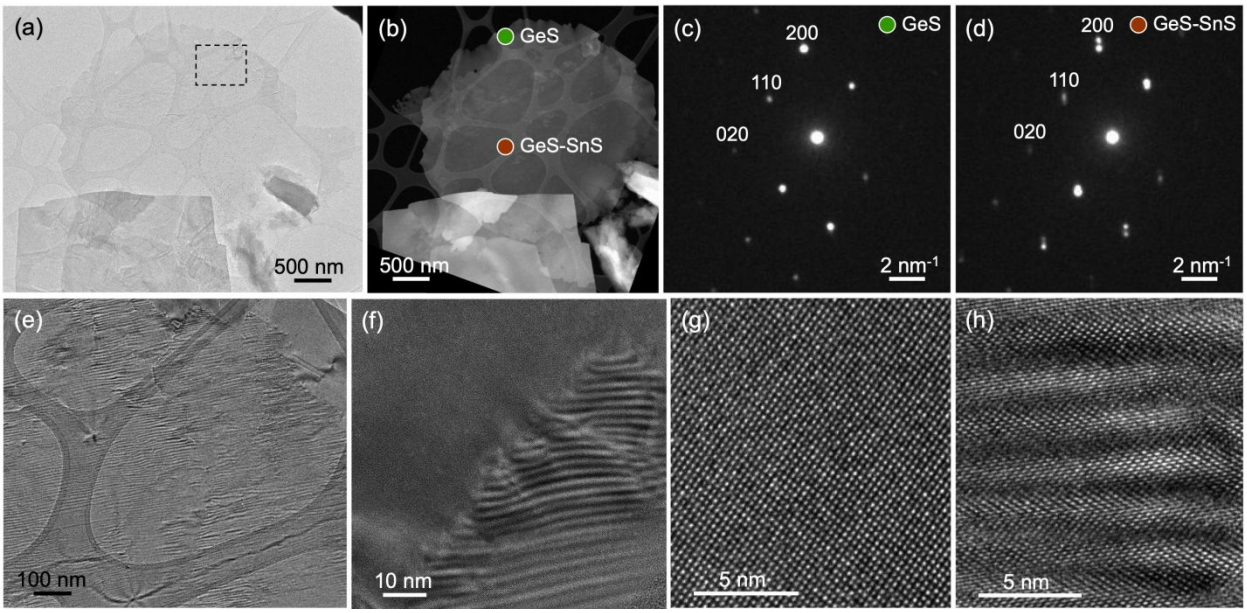

Figure S4. Morphology of thin GeS-SnS heterostructures. (a) TEM, **(b)** HAADF-STEM images of a characteristic thin GeS-SnS heterostructure (GeS source temperature: 400°C). **(c)**, **(d)** Nanobeam electron diffraction pattern from the GeS edge band and the center of the heterostructure (as marked in (b)). Zone axis: [001]. **(e)** Higher magnification TEM image of part of the flake marked by a rectangle in (a), showing a continuous moiré pattern across the central region. **(c)** Detail of the lateral interface between the GeS-SnS center (identified by the moiré**,** right) and the GeS edge (moiré-free, left). **(g)**, **(h)** High-resolution TEM images of the GeS edge and the GeS-SnS center.

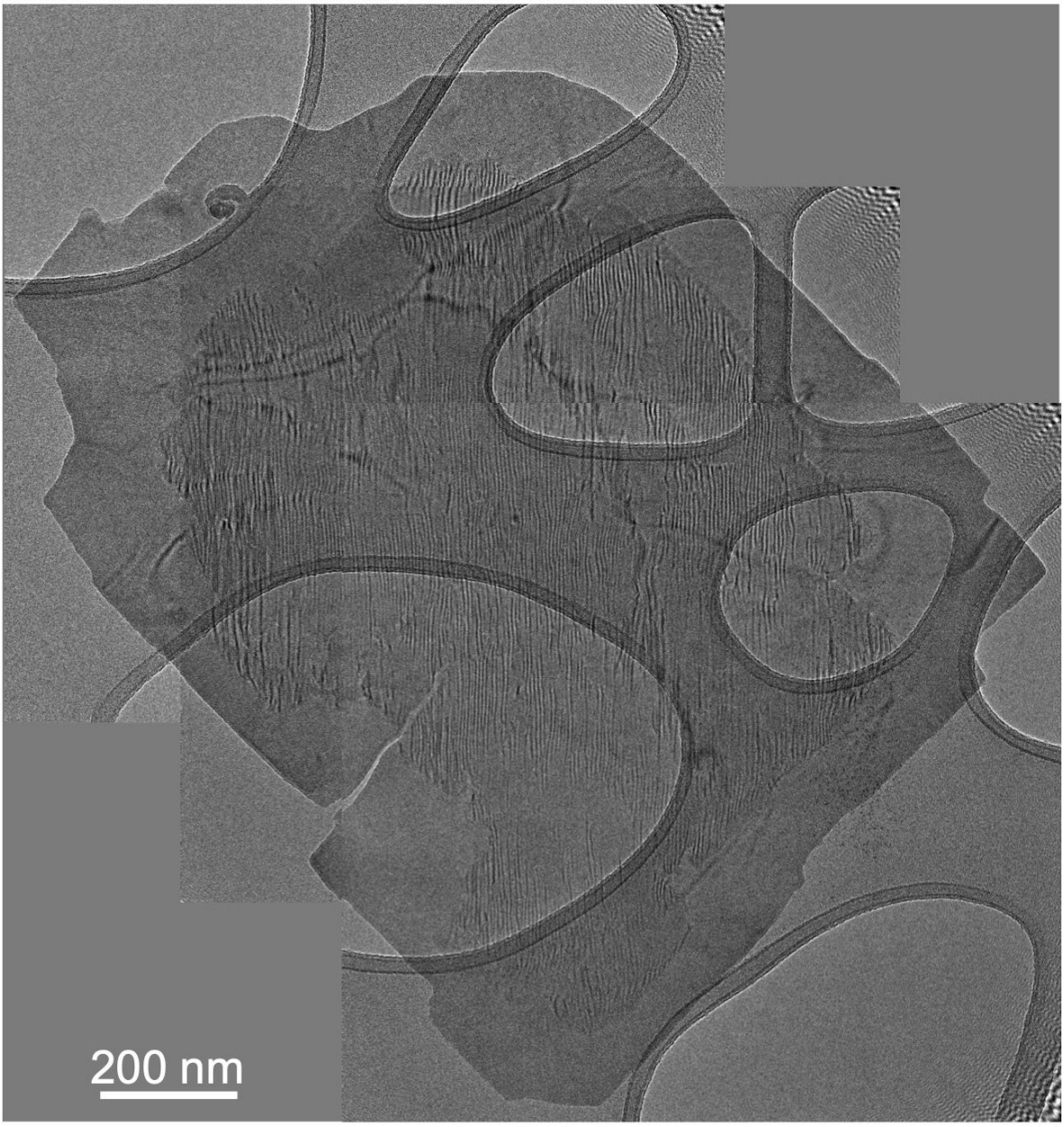

Figure S5. Stripe moiré pattern marks the extent of the central region with vertical GeS-SnS van der Waals heterostructure. Composite TEM image showing a thin GeS-SnS heterostructure. The GeS edge band is clearly distinguishable from the central GeS-SnS van der Waals stack by the presence of a stripe moiré pattern in the center and absence of the moiré near the edge.

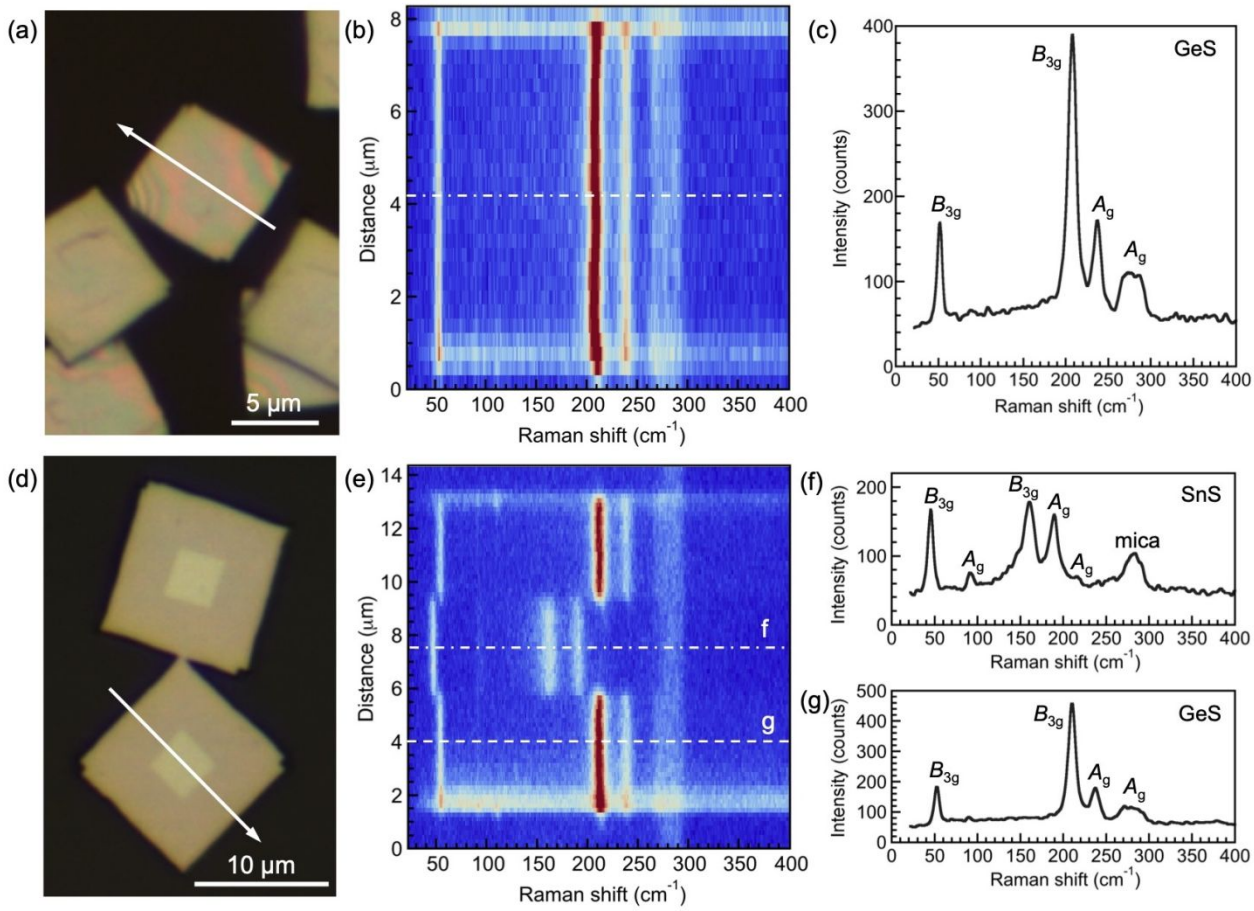

Figure S6. Raman analysis of characteristic GeS-SnS heterostructures grown from GeS precursor held at 450ºC. Measurements of the top of the heterostructures: (a) Optical microscopy of GeS-SnS flakes on the original mica substrate. **(b)** Raman linescan across one of the flakes shown in (a). **(c)** Raman spectrum showing GeS signal throughout the entire flake. **Measurements of the bottom of the heterostructures: (d)** Optical image of typical GeS-SnS heterostructures, supported by a PDMS stamp and exposing their bottom surfaces that were in contact with the mica substrate. **(e)** Raman linescan across one of the flakes shown in (d). The residual mica signal (280-290 cm^{-1}) originates from a thin layer of the van der Waals substrate that was transferred to the stamp along with the GeS-SnS flakes. **(f)**, **(g)** Raman spectra from the GeS-SnS center (dash-dotted line in (e)) and the wide GeS edge of the heterostructure (dashed line in (e)), respectively.

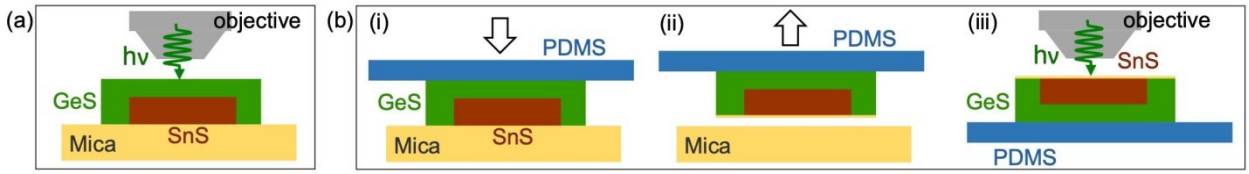

Figure S7. Schematic of the dry transfer to measure GeS-SnS heterostructures from the bottom side. (a) Conventional optical microscopy and Raman spectroscopy on the mica growth substrate. **(b)** Lift-off of heterostructure flakes using a PDMS stamp, and optical measurements from the bottom side of the flakes.

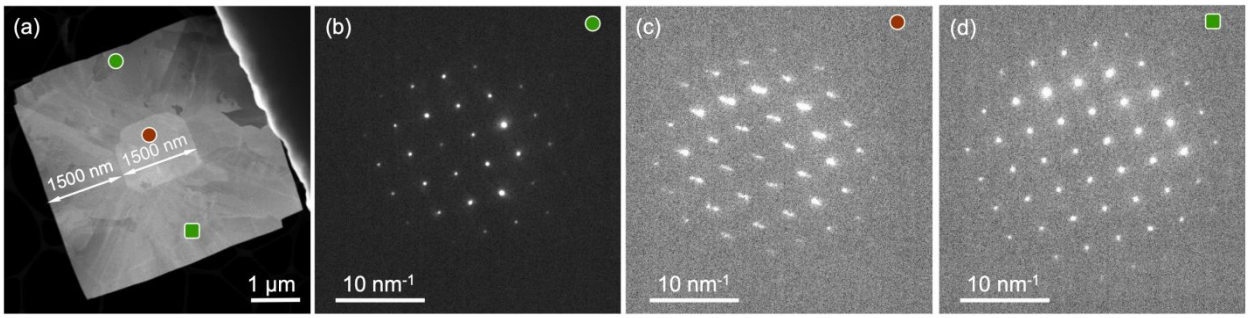

Figure S8. Morphology of GeS-SnS heterostructure grown from GeS precursor held at 450ºC. (a) HAADF-STEM image of a characteristic GeS-SnS flake, similar to the flakes shown in Figure S4. **(b)-(d)** Nanobeam electron diffraction patterns at different positions of the heterostructure, as marked in (a).

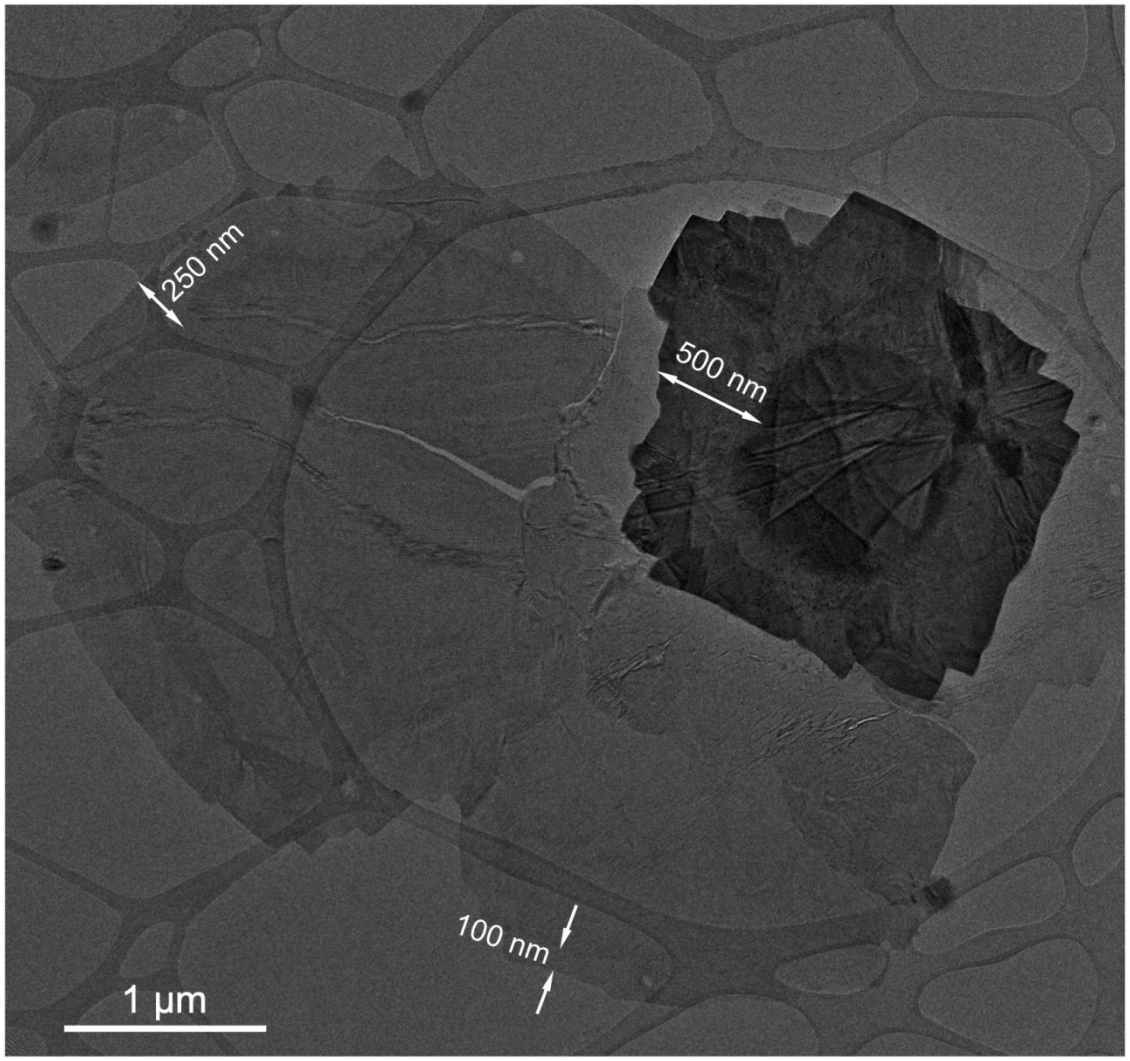

Figure S9. GeS edge width in GeS-SnS heterostructures with different thickness. TEM image comparing three characteristic GeS-SnS heterostructures with different thickness of the original SnS flakes, grown under the same conditions (GeS source temperature: 400ºC). The GeS edge width decreases with decreasing SnS flake thickness.

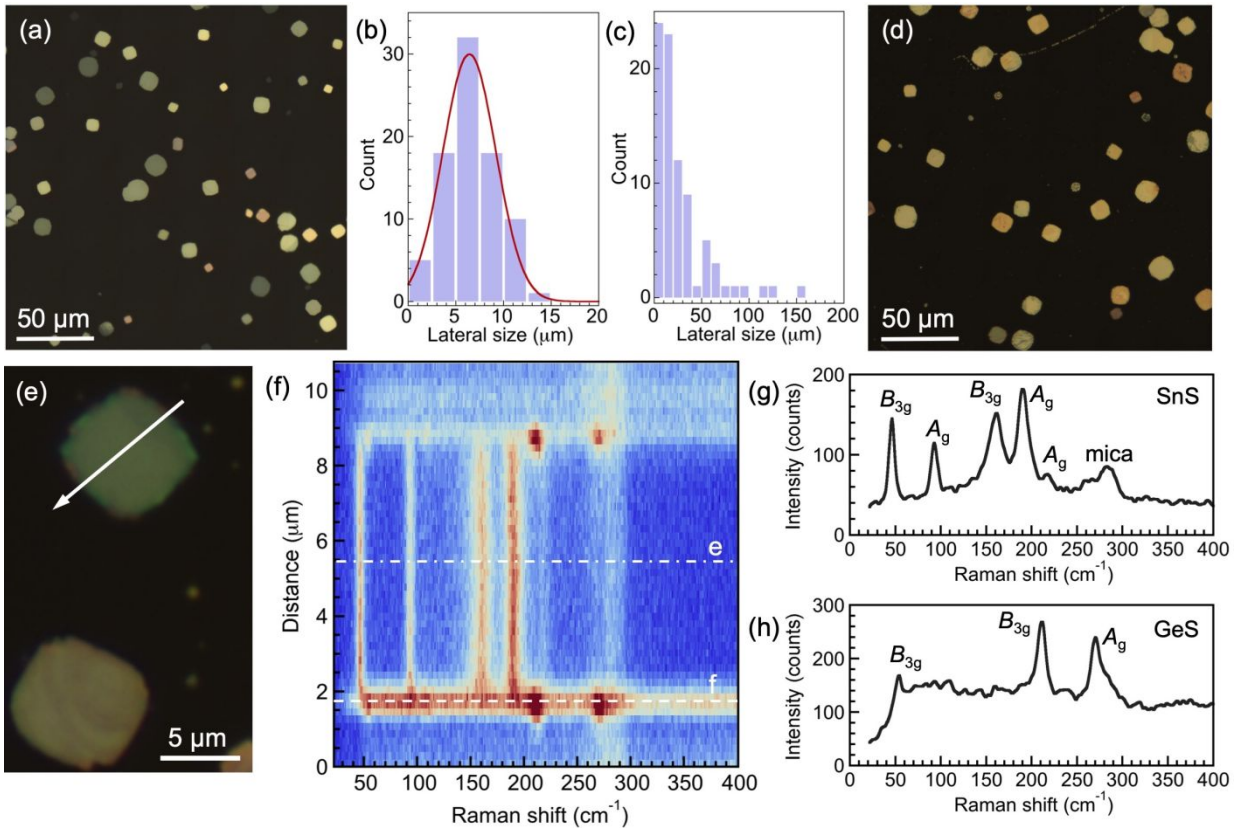

Figure S10. GeS-SnS heterostructures formed from thin SnS flakes. (a) Optical microscopy image of thin SnS flakes on mica substrate. Note the characteristic microfaceted, rounded (rather than rhombic) shape observed for thin SnS flakes. **(b)** Histogram of lateral sizes of the thin SnS flakes, obtained from AFM measurements. Red line: Gaussian fit showing a mean lateral size of 6.4 μm. **(c)** Thickness histogram of the thin SnS flakes, obtained from AFM measurements. Note the pronounced peak at thickness below 50 nm. **(d)** Image of a different region of the same sample following GeS growth. **(e)** Higher magnification optical image of a characteristic GeS-SnS heterostructure. **(f)** Raman linescan across one of the flakes shown in (c). **(g)**, **(h)** Raman spectra from the GeS-SnS center of the heterostructure and the narrow GeS edge, respectively.

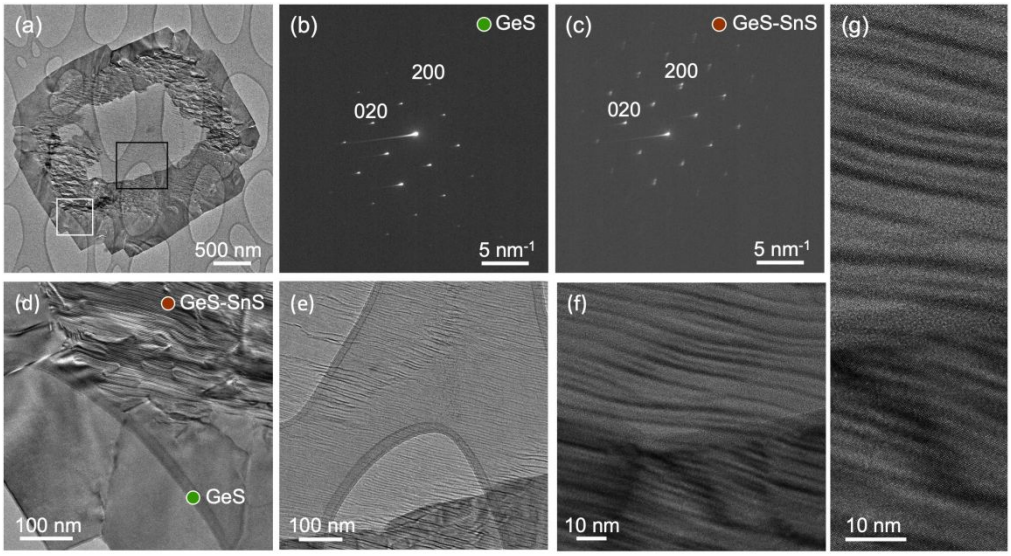

Figure S11. Morphology of a GeS-SnS heterostructure in which part of the SnS center has been exfoliated during transfer to a TEM support. (a) TEM image of a characteristic GeS-SnS flake with partially removed central region. **(b)** Electron diffraction pattern from the GeS edge. Zone axis: [001]. **(c)** Nanobeam electron diffraction from the center of the flake showing the superposition of the GeS and SnS reflections after the thinning of the SnS in the center. **(d)** Higher magnification TEM image of the interface between the GeS edge and the moiré superlattice in the GeS-SnS center (white rectangle in (a)). **(e)** TEM image showing moiré fringes in the area where part of the SnS was removed (black rectangle in (a)). While the persistent moiré pattern demonstrates stacked GeS-SnS, the lighter contrast of the center compared to the GeS edge clearly shows that vertically grown GeS layer is much thinner that the laterally grown GeS of the edge. **(f)**, **(g)** High-resolution TEM images of the moiré fringes in the center of the heterostructure.

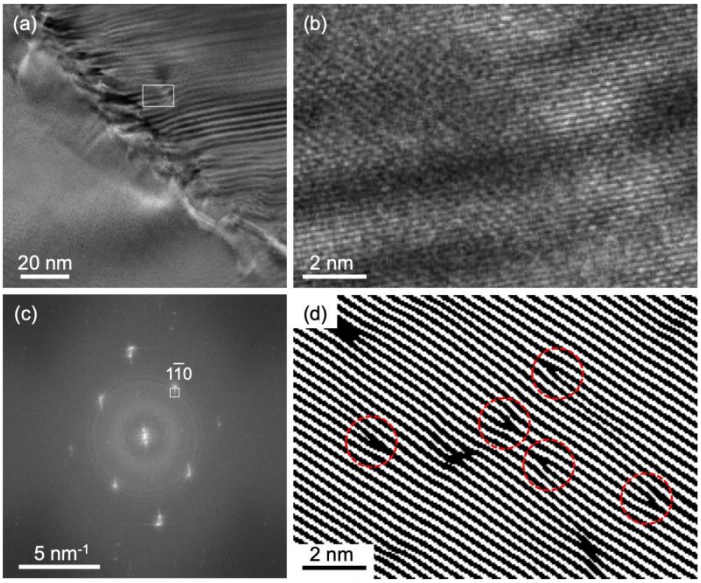

Figure S12. Dislocations near the lateral GeS-SnS interface. (a) HRTEM image obtained near the lateral interface of a GeS-SnS heterostructure. **(b)** Magnified view of the area marked by a rectangle in (a). **(c)** FFT power spectrum of the HRTEM image shown in (a). **(d)** Image (b), Fourier-filtered with portion of the $1\bar{1}0$ spot marked in (c). Red circles indicate edge dislocations in the image.

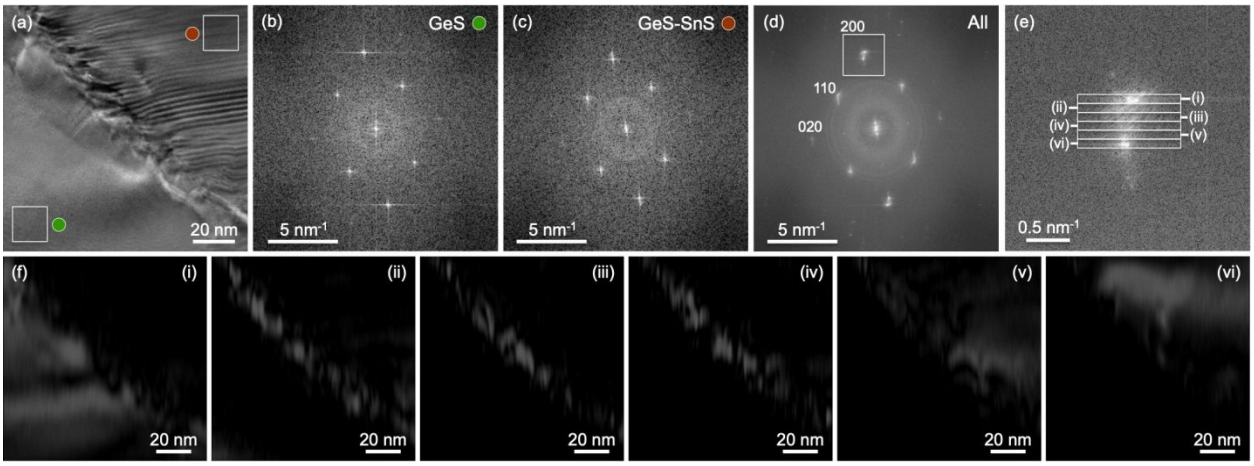

Figure S13. Fast-Fourier transform (FFT) analysis of *a*-lattice constants from HRTEM near the interface. (a) HRTEM image obtained near the interface of a GeS-SnS heterostructure. Moiré free parts (lower left) correspond to the GeS edge; regions with stripe moiré mark the GeS-SnS vertical heterostructure. **(b)** FFT power spectrum from the lower left rectangle in (a), showing GeS reciprocal spots. **(c)** Power spectrum from the upper right rectangle in (a), showing relaxed GeS and SnS. **(d)** FFT power spectrum of the entire area shown in (a). **(e)** Detail of the (100) spot, with marked rectangular areas ((i) through (vi)) from which inverse-FFT images were obtained. Region (i) corresponds to a^{GeS}, while region (vi) corresponds to a^{SnS}. **(f)** Fourier-filtered images from reciprocal space regions (i) through (vi) marked in (e).

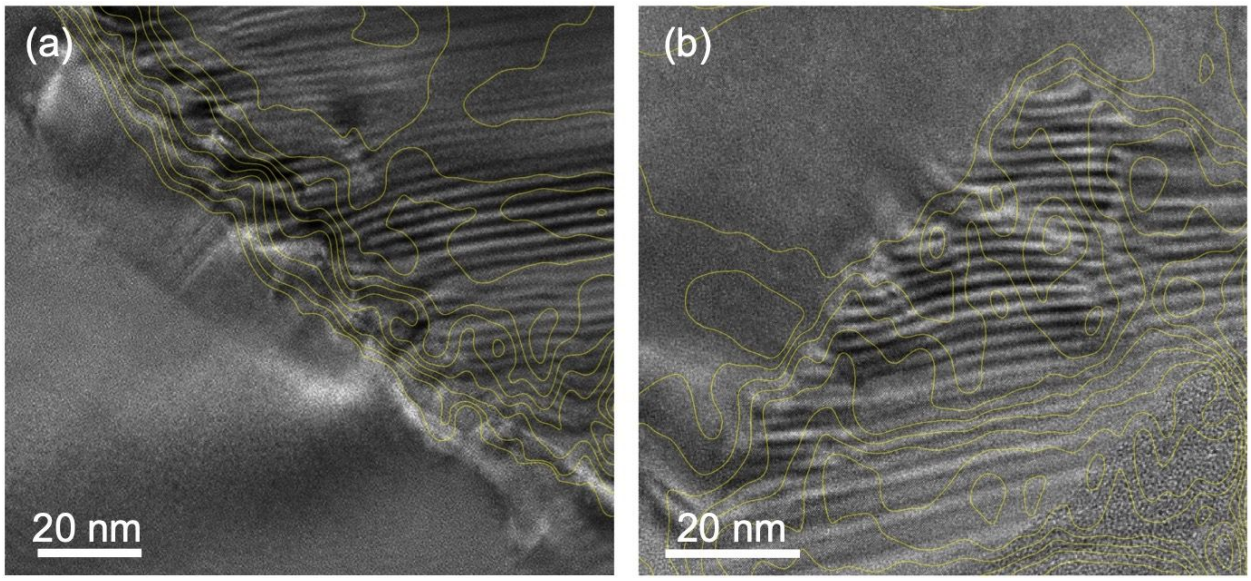

Figure S14. Alloyed region and stripe moiré pattern at the lateral interface. (a) HRTEM image and contours of the gradually changing *a* lattice constant across the interface for the thick heterostructure shown in Figure 3 (a)-(c). **(b)** HRTEM image and contours of the gradually changing *a* lattice constant across the interface for the thin heterostructure shown in Figure 3 (d)-(f).

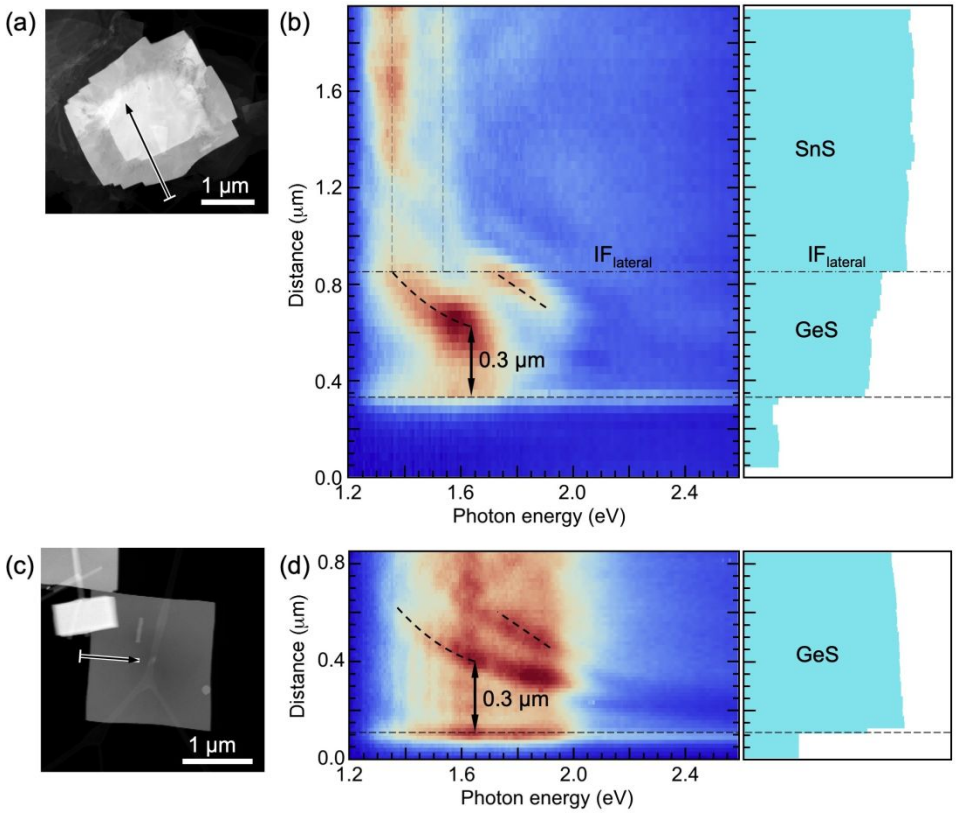

Figure S15. Waveguide mode interference in GeS-SnS heterostructures and GeS flakes. (a) HAADF-STEM image of the GeS-SnS heterostructure shown in Figure 4. **(b)** (Left) Hyperspectral STEM-CL linescan along the arrow shown in (a); (right) corresponding STEM intensity, showing the position of the flake edge and lateral GeS-SnS interface ($IF_{lateral}$). **(c)** HAADF-STEM image of a pure GeS flake. **(d)** (Left) Hyperspectral STEM-CL linescan along the arrow shown in (c); (right) corresponding STEM intensity, showing the position of the flake edge. Dashed lines in (d) mark the dispersion of fringes due to constructive interference of the primary luminescence with waveguide modes reflected from the flake edge. While there are differences in the intensity distribution, the same dispersive fringes are found in the GeS edge band of the GeS-SnS heterostructure.

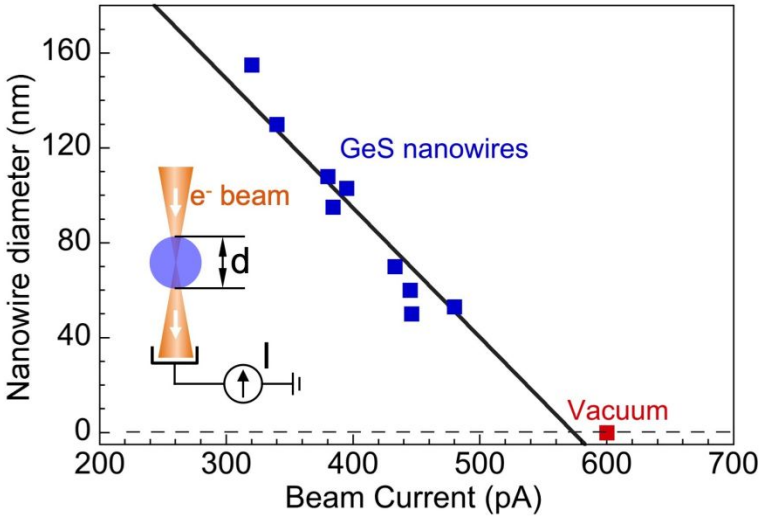

Figure S16. Determining the (vertical) thickness of the GeS edge band from electron beam current attenuation. Measurements of the electron beam current on suspended GeS nanowires with different diameters (d, blue symbols) in comparison with the beam current measured in vacuum (without a sample, red symbol), used to calibrate the attenuation of the electron beam current as a function of GeS thickness. The inset shows a schematic of the measurement, in which the electron beam after traversing the sample is collected by a Faraday cup and its current (I) measured by a pico-ampere meter.